The deformation and work hardening behaviour of a SPD processed Al-5Cu alloy

Hailong Jia[a], Ruben Bjørge[b], Knut Marthinsen[a], Yanjun Li[a,*]

[a] Department of Materials Science and Engineering, Norwegian University of Science and Technology (NTNU), 7491 Trondheim, Norway

[b] SINTEF Materials and Chemistry, 7465 Trondheim, Norway

***Corresponding author: yanjun.li@ntnu.no (Y.J. Li).**

Abstract

An Al-5 wt.% Cu alloy supersaturated with Cu in solid solution was subjected to equal channel angular pressing (ECAP). The microstructural evolution was systematically investigated by backscattered electron (BSE) imaging, electron backscatter diffraction (EBSD) and transmission electron microscopy (TEM). It is revealed that a bimodal grain structure composed of coarse micron-sized grains and submicron-sized grains was developed after four passes of ECAP. Tensile testing showed that a high ultimate tensile strength of ~500 MPa, a high elongation to failure of ~28% and a uniform elongation of ~5% were achieved simultaneously. The deformation behaviour and the grain structure evolution during ECAP, the strengthening mechanisms of the as-deformed material, and especially, the role played by a high content of Cu have been discussed.

Keywords: Aluminium alloy; ECAP; Bimodal grain structure; Tensile properties

1. Introduction

Al-Cu alloys are one of the most important high strength aluminium alloys and employed extensively in structural applications. The as-cast microstructure of Al-Cu alloys with a high content of Cu is usually composed of aluminium matrix supersaturated with Cu solutes and coarse eutectic θ particles (Al_2Cu) distributed along grain boundaries. Usually, a solution heat treatment followed by an age hardening treatment has to be conducted to achieve the high strength for these alloys. Severe plastic deformation (SPD) methods, particularly, equal channel angular pressing (ECAP), have been widely used to produce bulk ultrafine grained (UFG) and nanocrystallined (NC) metals and alloys with superior strengths [1-5]. However, most of the UFG and NC materials show rather limited ductility at room temperature, where the elongation to failure is just a few percent and the uniform tensile elongation is even smaller [6]. This is

attributed to the low work hardening rate of the materials, which is a result of low dislocation accumulation capability of the submicron-sized and nano-sized grains. The poor ductility of UFG materials processed by SPD limits their further deformation and application potentials. So far, different strategies have been proposed to improve the ductility of UFG and NC materials, e.g. the introduction of a fine dispersion of nanoparticles or twin boundaries into the nanostructured matrix [7, 8] and the generation of bimodal grain structures [9-12]. Among these approaches, generating bimodal grain structures is proved to be the most promising one. Recently, by using this strategy, high strength (~507 MPa) and large uniform elongation (~11%) were achieved simultaneously in a binary Al-7 wt.% Mg alloy processed by room temperature ECAP (RT-ECAP) [13, 14]. The formation of the bimodal grain structure was attributed to the high content of Mg in solid solution. Firstly, a high Mg solute content increases the atomic friction of dislocation slips, which resulted in inhomogeneous deformation behaviours of coarse grains with different orientations. Secondly, the high Mg solute content also strongly supressed the rearrangement of diffuse dislocation boundaries into subgrain boundaries and high angle boundaries (HABs).

In aluminium alloys, solute Cu has an even stronger work hardening effect than Mg in aluminium alloys. It is therefore expected that a high solute content of Cu also favours the generation of a bimodal grain structure in Al-Cu alloys subjected to SPD and thus possibly enhances the ductility. However, most Al-Cu alloys (containing 2-4 wt.% Cu) subjected to RT-ECAP show a uniform grain structure and they have an ultimate tensile strength (UTS) of ~290-450 MPa and a uniform elongation (ε_u) of ~1-4% [15-18]. Studies on RT-ECAP of Al-Cu alloys containing higher levels of Cu content have been few and no bimodal grain structures have been reported. Tensile properties of an ECAP processed Al-5 wt.% Cu (through a 110˚ die via route A, i.e. no billet rotation between passes) was studied in Ref. [19], in which an UTS of ~493 MPa with a low elongation to failure value (less than 10%) was achieved after 8 passes.

The aim of the present work is to explore the possibility to achieve a bimodal grain structure in Al-Cu alloys with high strength and improved ductility by exploiting the high work hardening potential of Cu. Different strategies have been applied to promote the heterogeneous deformation during ECAP. Firstly, an Al-5 wt.% Cu alloy after solution treatment and quenching was used. This alloy contains a small fraction of coarse eutectic Al_2Cu particles, which cannot be dissolved into the matrix during a homogenization treatment. The presence of coarse particles can enhance the formation of ultrafine grains around the particles due to particle stimulated continuous dynamic recrystallization (CDRX) during ECAP [20, 21].

Secondly, ECAP via route A in a 90˚ die was applied. Such a process route will ensure that a fraction of coarse grains can be subjected to less deformation due to the unfavourable orientations. The microstructural evolution, the deformation and grain refinement mechanisms of the Al-5Cu alloy during ECAP, and the mechanical properties of as-deformed samples were systematically investigated.

2. Experimental Procedure

A binary Al-5 wt.% Cu alloy prepared by using commercial purity Al and high purity Cu was used in the present work. Prior to ECAP, Al-5Cu bars with dimensions of 100 mm × 19.5 mm × 19.5 mm were homogenized in a salt bath furnace at 540 ˚C for 24 h followed by water quenching. Then, these bars were subjected to ECAP through a 90˚ die via route A at room temperature, which leads to an imposed equivalent strain of about 1.0 per pass [22]. To lower the friction during pressing, samples were coated with a thin layer of graphite lubricant. The ECAP samples were processed for various numbers of passes through the die, up to a maximum of four. A sample that had gone through X (here X = 1, 2, 3 and 4) passes of ECAP was labelled as XP sample.

Samples for microstructure characterization, hardness and tensile test measurements were cut from the uniformly deformed regions of the ECAP processed bars. BSE images and EBSD data were obtained from the longitudinal sections of the samples. After standard mechanical grinding and polishing, ion milling at 3.5V for 45 min was carried out on the surface of EBSD samples. EBSD was conducted in a Hitachi SU-6600 field emission gun-scanning electron microscope (FEG-SEM) equipped with a Nordif EBSD detector and TSL OIM software. Thin foils for transmission electron microscopy (TEM) were prepared by twin-jet electropolishing in a solution of 33% nitric acid in methanol at -30 ˚C. TEM observation and TEM orientation mapping were carried out using a JEOL 2010F TEM operated at 200 kV, equipped with the NanoMegas ASTAR system for scanning precession electron diffraction (SPED). Mechanical properties were evaluated by both hardness and tensile testing. Vickers hardness measurements were performed using a DVK-1S Vickers hardness testing machine under a load of 1 Kg applied for 15 s. The hardness values reported were an average of at least ten separate measurements. Tensile test specimens were machined from the ECAP bars in the longitudinal direction, with a gauge length of ~8 mm, width of ~4 mm and thickness of ~2 mm. Tensile tests were conducted at room temperature and a strain rate of $5 \times 10^{-4} s^{-1}$, using a MTS 810 hydraulic universal testing machine with a 100 KN capacity.

3. Results and discussion

3.1. Microstructure evolution

3.1.1. Initial microstructure of Al-5Cu before ECAP

The microstructure of the as-homogenized material was examined by BSE and EBSD (Fig. 1). The initial microstructure consists of α-Al grains with an average size of ~40 μm and a small fraction of eutectic Al_2Cu particles with an average equivalent circular diameter of ~3 μm. Most of the Al_2Cu particles are located along grain boundaries and the area fraction of these particles is measured to be ~0.4% by using the software Image J.

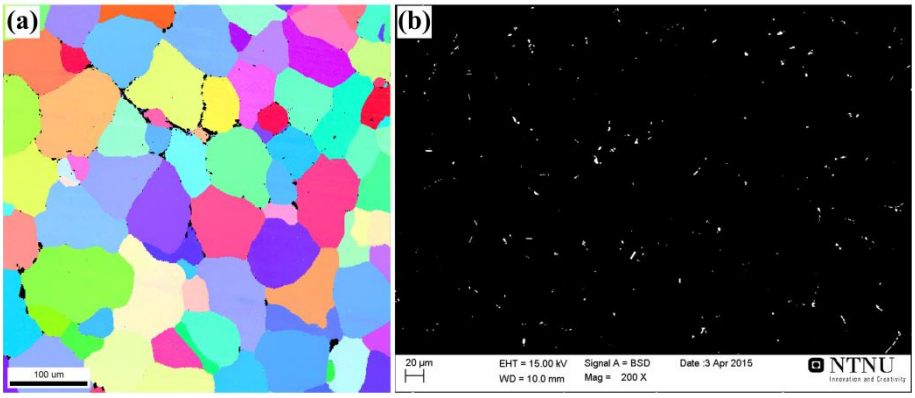

Fig. 1. Microstructures of the original as-homogenized Al-5Cu alloy: (a) EBSD map and (b) BSE map.

3.1.2. Microstructure of Al-5Cu processed by ECAP

Fig. 2(a) is a BSE image showing the deformation structure of the 1P sample. After one pass of ECAP, elongated grains have formed due to the severe shear deformation during ECAP. Most of the elongated grains are mainly aligned at an angle of ~30˚ to the extrusion direction (ED), which is well consistent with the previous analysis [15]. Inside the elongated grains, parallel slip bands can be frequently observed, for example, within the grain GI indicated by the white oval circle. In order to further investigate the deformation behaviour of the grains, EBSD was conducted on the same area of the BSE sample corresponding to the white rectangle in Fig. 2(a). The corresponding EBSD image is shown in Fig. 2(b). As can be seen, low angle boundaries (LABs), high angle boundary (HAB) segments and fine grains have also formed within some of the elongated grains. For the grain labeled GI, only alternating micro-bands with slight orientation differences can be observed. Fig. 2(c) shows a magnified EBSD image of the highlighted grain GI. Inside the grain, the boundaries between the micro-bands are diffuse and the point-to-point misorientations are mostly less than 4˚. Moreover, more LAB segments with higher misorientation angles

of 5-15° can also be observed in the vicinity of the original HABs than in the interior of the grain, which may be related to the more severe local deformation at the original HABs and around the coarse Al_2Cu particles [21]. The presence of diffusive boundaries can be attributed to the pinning effect caused by the high content of Cu in solid solution, which can strongly retard the migration of dislocations. Thus, the evolution of diffuse dislocation boundaries into regular subgrain boundaries through rearrangement of intrinsic dislocations by climb and/or cross slip becomes difficult. A similar diffuse micro-band boundary structure was also reported in an Al-7Mg alloy subjected to ECAP [13]. From the inserted point-to-origin misorientation profile along the elongated direction of the grain GI, a large long-range misorientation gradient exists in the elongated grain, indicating a high dislocation density in the grain.

Fig. 2(d) shows a magnified EBSD image of another isolated elongated grain, GII. As can be seen, even in the same grain the deformation is heterogeneous. In the upper left part of grain GII, there are mainly only micro-bands with misorientation angles less than 5°, while in the lower part a large number of sharp LABs with misorientation angles of 5-10° have formed. Again, one can see that the LABs tend to initiate from the original grain boundaries due to severe deformation around Al_2Cu particles [21] and the original HABs. As shown by the misorientation profile, a long-range misorientation gradient also exists in this grain. As exemplified by grains GI and GII, after one pass of ECAP, most of the elongated grains have only micro-bands but not any well-developed subgrain and cell structures. This should be related to the high Cu solute content [23] that strongly increases the critical shear stress of dislocation slips and therefore enhances the planar slip behavior [24, 25]. With few active dislocation slip systems, it is difficult to form 3D dislocation networks and therefore regular cell boundaries.

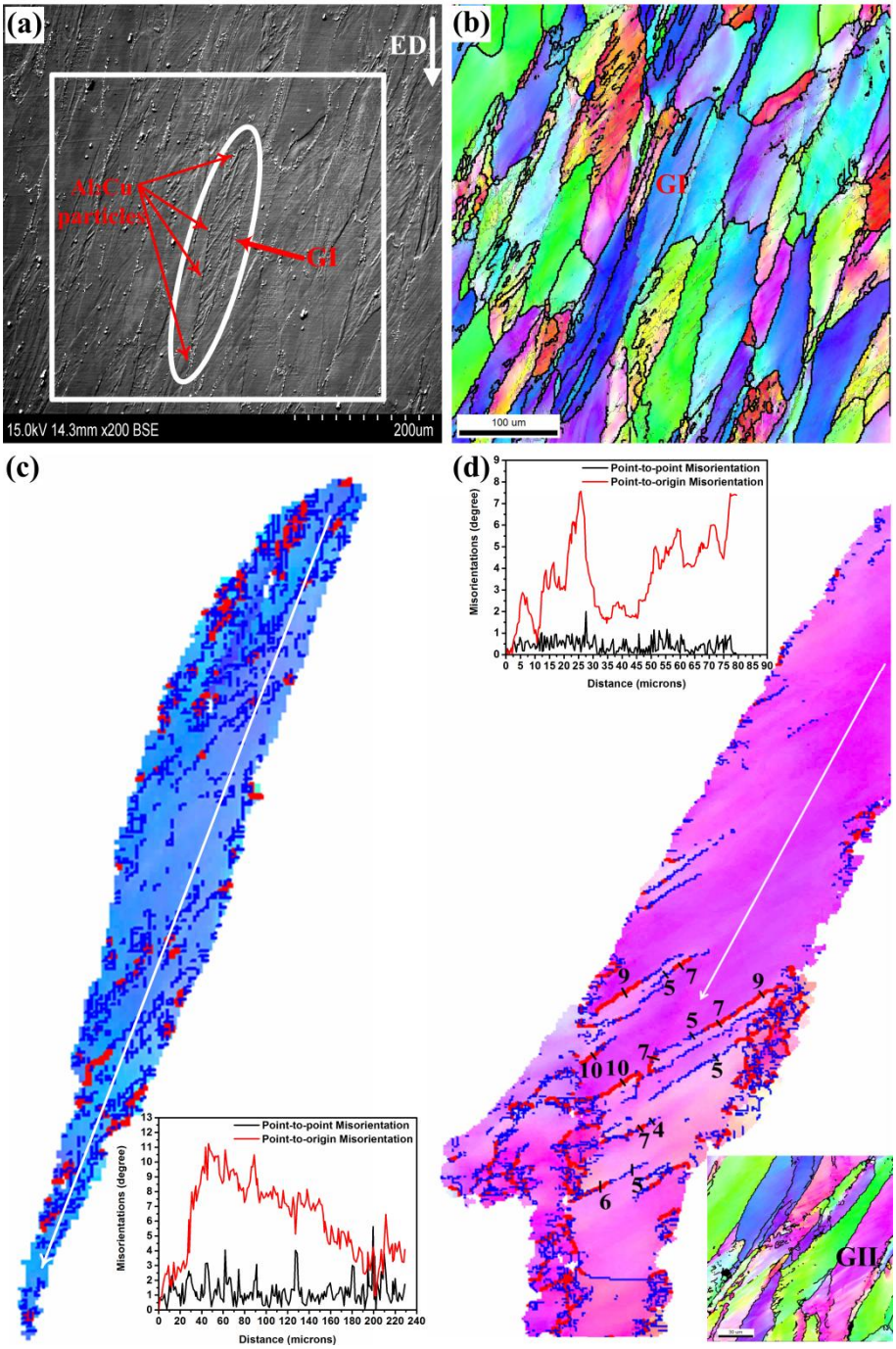

Fig. 2. Microstructures of the 1P sample: (a) BSE image; (b) EBSD image corresponding to the area within the white rectangular frame in (a); (c) enlarged EBSD image of the selected grain GI, showing diffuse boundaries; (d) selected grain GII, showing micro-bands inside of the grain. Corresponding misorientation profiles measured along the lines are also included. Inside of GI and GII, the blue and red lines depict differences between neighbouring grid points $2^\circ < \Theta \leq 5^\circ$ and $5^\circ < \Theta \leq 15^\circ$ respectively.

Fig. 3 shows the BSE and corresponding EBSD images of the 2P, 3P and 4P samples. EBSD analysis was done on the areas highlighted by rectangular frames in the BSE images. After two passes (Fig. 3(b)), the width of the coarse elongated grains are further reduced. Besides, a comparison between the BSE (Fig. 3(a)) and EBSD image (Fig. 3(b)) shows that a large number of fine equiaxed grains have formed along

HABs and at the triple junctions of the coarse grains, which can be related to the presence of eutectic Al_2Cu particles.

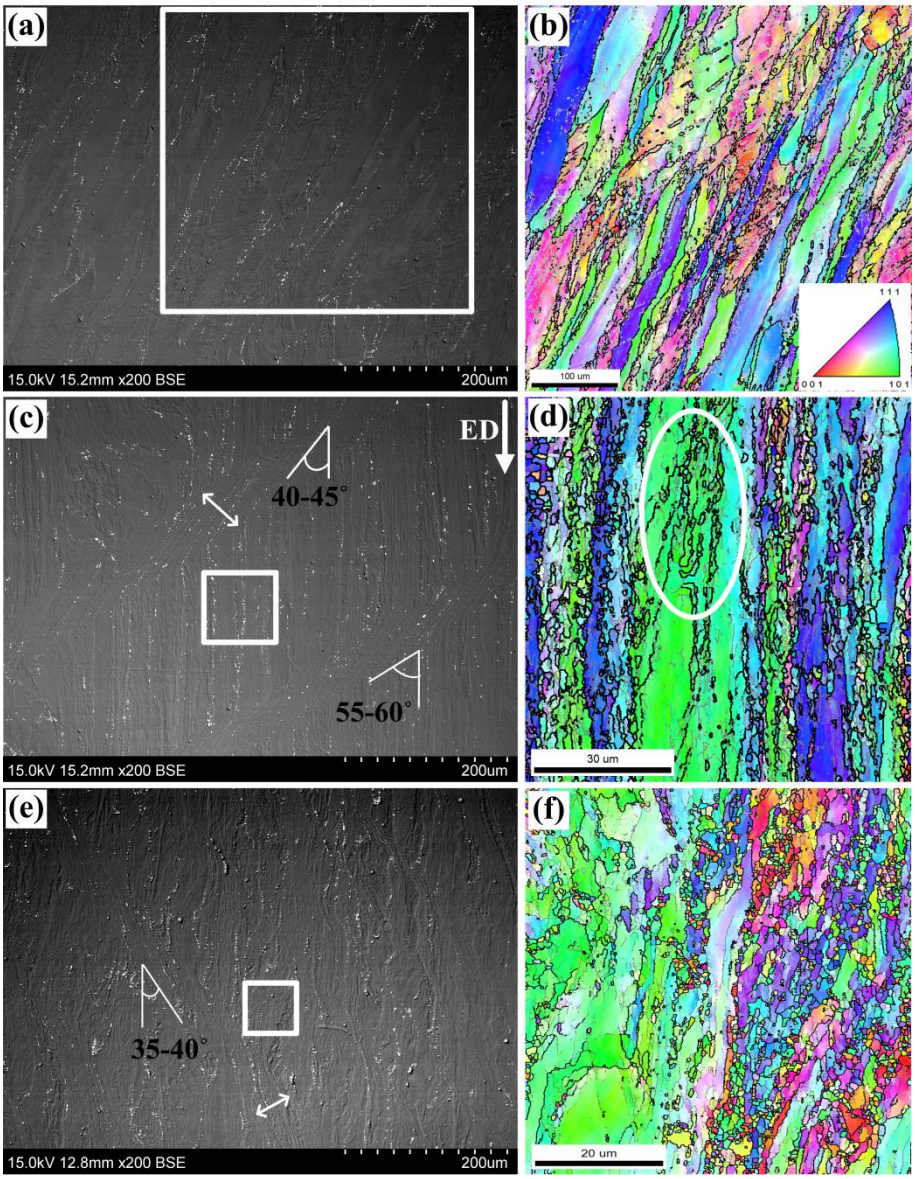

Fig. 3. Typical BSE images, and corresponding EBSD maps of the areas indicated by rectangular frames in the BSE images. (a) and (b) 2P; (c) and (d) 3P; (e) and (f) 4P. The white dots in the BSE images are eutectic Al_2Cu particles. In the EBSD maps, narrow grey and coarse black lines depict differences between neighbouring grid points $5^\circ < \Theta \leq 15^\circ$ and $15^\circ < \Theta \leq 180^\circ$ respectively.

From Fig. 3(c) and (e), it can be seen that after three and four passes, a large fraction of shear bands has formed. The formation of shear bands is common for Al alloys containing high levels of solutes when subjected to large deformations. The angles between the shear band structures and ED are in the range 35-60° (as exemplified by the white markings in Fig 3(c) and (e)). The widths of the shear bands after three and four passes are 30-40 μm and 20-30 μm, respectively.

From the EBSD image shown in Fig. 3(d), it can be seen that more equiaxed ultrafine grains have formed inside the coarse grains and along the HABs of elongated grains. Interestingly, there are less UFG equiaxed grains inside the green coarse grains than grains indexed with other orientation colors, implying a less deformation extent in this grain. This is also true for the green color grains in 4P sample (Fig. 3(f)). A shear factor [26] calculation for the green coarse grain marked by an oval circle shows that it has only two slip systems with shear factor values larger than 0.5 (i.e., 0.97 and 0.55). Because of the limited active slip systems in these grains, subdivision of such coarse grains into fine subgrains and subsequently their further transformation into grains delimited by HABs is difficult. A careful examination reveals that many of the equiaxed fine (sub)grains inside coarse grains are surrounded by HAB segments connected to LAB segments (as indicated by the oval circle in Fig. 3(d)). This observation indicates that the fine and UFG equiaxed grains have formed by CDRX via transformation of LABs into HABs with increasing misorientation angles of subgrain boundaries during ECAP, which greatly contributes to the refinement of coarse grains.

As shown in Fig. 3(f), there is a large fraction of submicron-sized ultrafine equiaxed grains in the 4P sample. However, coarse micron-sized grains can still occasionally be observed, which means that a bimodal grain structure has formed. This is similar to the bimodal grain structure obtained in an ECAP processed Al-7Mg alloy after a strain of ~3 [13]. The existence of the coarse micro-sized grains is mainly attributed to their unfavorable grain orientations that make the activation of multi-dislocation slips difficult during ECAP. Since route A is used, the shear factor of the coarse grains has a limited change from pass to pass. The subdivision of those coarse grains with an unfavorable orientation is thus difficult even when subjected to higher deformation strains (i.e. more ECAP passes).

Inside the large grains in the 4P sample, the density of geometrically necessary dislocations can roughly be estimated by the misorientation gradient according to the equation $\rho \approx {}^{\theta}/_{b\delta}$ [13], where θ is the accumulated misorientation angle in radians within a distance δ, and b is the Burgers vector. With $b = 2.86 \times 10^{-10}$ m for pure Al and values for θ and δ derived from the misorientation profiles in different large grains in Fig. 3(f), the local dislocation density is estimated to be ~1-2 $\times 10^{14}$ m^{-2}, which is comparable to typical values of dislocation density in the heavily deformed Al-7Mg alloy [13].

Fig. 4(a)~(c) show the evolution of the measured average crystallite size, fraction of different types of boundaries and average misorientation of ECAP samples as a function of deformation strain. The average

width δ and length L were measured perpendicular to and parallel with the longitudinal direction of grains, respectively.

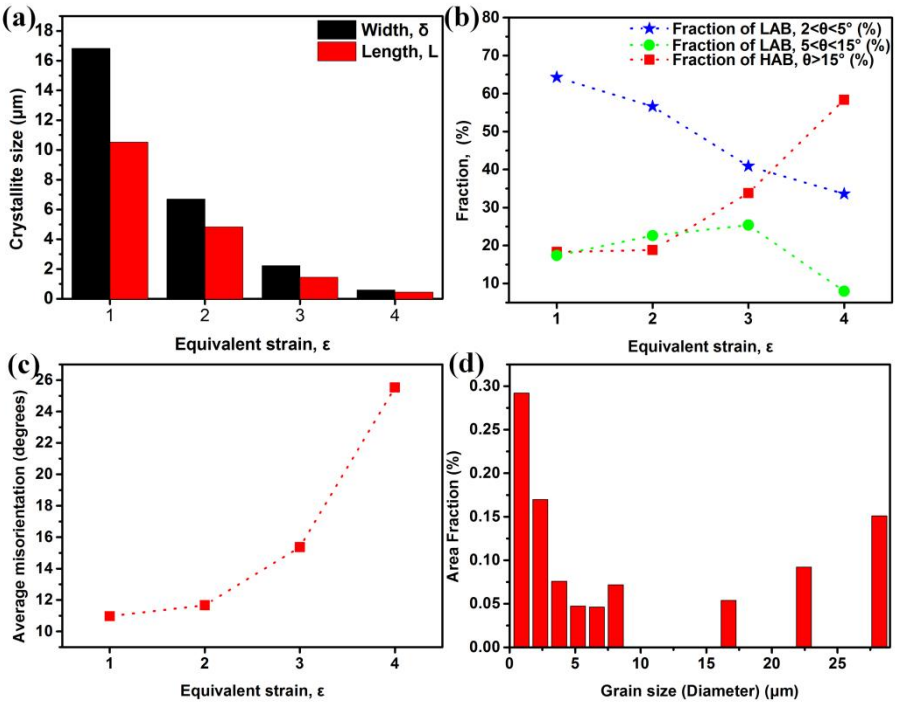

Fig. 4. The evolution of (a) the average crystallite size with boundary misorientation ≥5˚, (b) fraction of different types of boundaries and (c) average misorientation of boundaries as a function of equivalent deformation strain; (d) grain size distribution of the 4P sample.

There is a sharp decrease of average grain size after the first pass of ECAP, i.e. the length of grains reduces from ~40 μm to ~17 μm (Fig. 4(a)). The aspect ratio of the grains drops with increasing deformation strain. In the 4P sample, the average grain size is measured to be ~0.4 μm and ~0.65 μm for δ and L, respectively. As shown in Fig. 4(b), after two passes of ECAP, the grain boundaries are dominated with LABs with misorientation of θ≤5˚, while the fractions of HABs and LABs with 5<θ≤15˚ are low. This is consistent with the results shown by Fig. 2 and 3, where most of the LABs are in the range of θ≤5˚. The fraction of LABs with higher misorientation angles 5<θ≤15˚ increases with deformation strain, showing the increase of misorientation angles of LABs with deformation strain. From the 2nd to 4th pass of ECAP, there is a sharp increase for the fraction of HABs at the consumption of LABs. This is more significant during the 4th pass of ECAP which may be due to the saturation of dislocations in the alloy and the fast evolution of LABs into HABs by the CDRX process. The sharp increase of average misorientation of boundaries from the 3rd to 4th pass (Fig. 4(c)) shows the same trend.

Fig. 4(d) shows the crystallite size distribution histogram of the 4P sample based on the EBSD image in Fig. 3(d), indicating a bimodal grain structure. However, since good quality EBSD orientation maps can be obtained only in regions containing a considerable volume fraction of coarse grains while regions dominated by ultrafine grains appeared with poor Kikuchi patterns, the actual volume fraction of ultrafine grains is much higher than that indicated by Fig. 4(d). To further study the bimodal grain structure achieved in this alloy, TEM characterization and orientation mapping based on scanning precession electron diffraction (SPED) were carried out on the 4P sample. Fig. 5(a) shows the orientation map of a micron-sized coarse grain. Inside the coarse grain, LABs with misorientation angles of 6-14° and submicron-sized grains bounded by HABs can also be observed. Interestingly, many discontinuous HAB segments can be seen connecting with the LABs, clearly demonstrating the CDRX process. Fig. 5(b) shows a bright field TEM image of the framed area in Fig 5(a). As can be seen, there are many dislocation tangles inside the coarse grain, indicating a high density of dislocations. Fig. 5(c) shows the co-existing micron-sized coarse grains and UFG grains, both equiaxed and elongated. As can be seen, the equiaxed UFG grains preferentially form at the previous HABs of elongated coarse grains. In the sample, the lamellar structure that consists of elongated ultrafine grains of ~100 nm in width can also be frequently observed (Fig. 5(d)), which is similar to the microstructure obtained in the Al-4wt.% Cu alloy processed by ECAP via a 120° die through route A [27]. These elongated ultrafine grains have also a high density of dislocations.

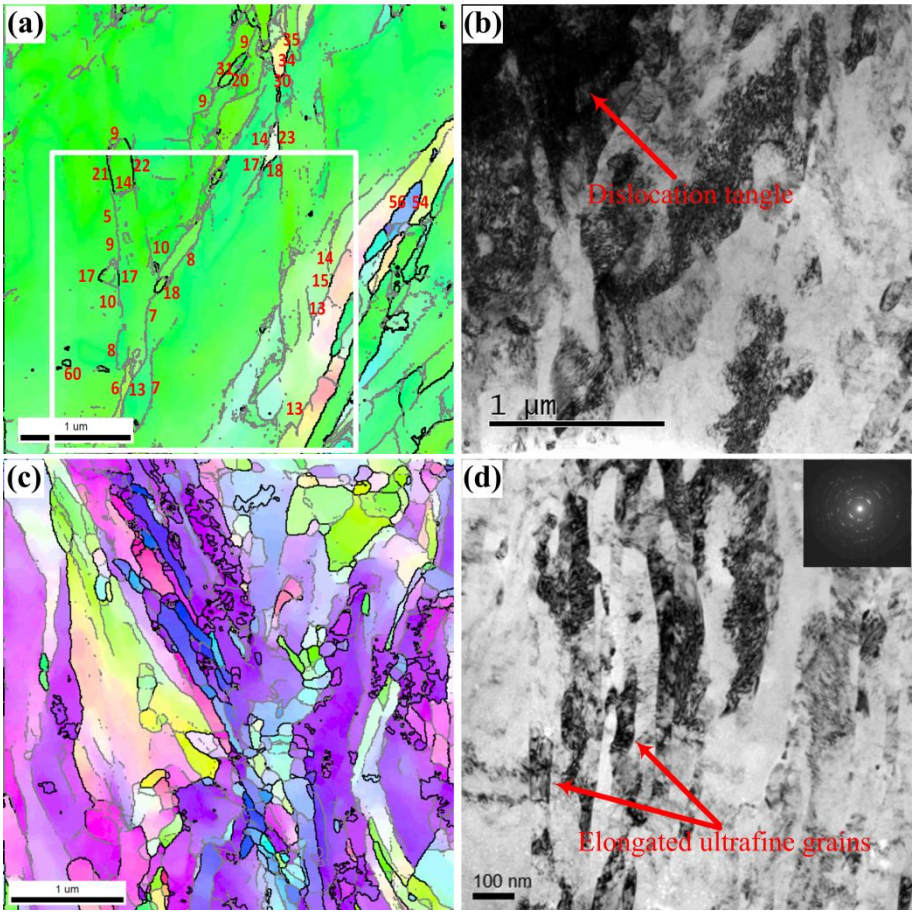

Fig. 5. (a) and (c) Typical ASTAR-TEM orientation images of the 4P sample and the step sizes are 10.2 nm and 9.0 nm, respectively. The narrow grey and coarse black lines depict LABs ($5^\circ < \Theta < 15^\circ$) and HABs ($15^\circ < \Theta < 180^\circ$), respectively. (b) and (d) Representative TEM images of the 4P sample, where (b) is taken from the framed area in (a).

The bimodal grain structure obtained in the present study is a result of incomplete CDRX that can be associated with the deformation behaviour of grains with different orientations. Non-uniform deformation can be attributed to the combined effect of a high content of Cu, the specific ECAP route used, the angle of ECAP die and the coarse particles. During shear deformation in ECAP, individual grains in the samples are not deformed uniformly due to the orientation difference. The high solute content of Cu increases the critical shear stress for activition of dislocation slips. At the same time, it suppresses the rearrangement of diffuse dislocation boundaries into subgrain boundaries. For the grains with unfavorable orientations, less dislocation slip systems are activated. Thus the coarse grains with unfavourable orientaions are difficult to be subdivided into fine grains by the development of subgrain boundaries. Different from the mostly used route Bc in ECAP, the relative change of shear direction to the grain orientation during ECAP via route A from pass to pass is limited, especially at higher pass numbers. This fact reduces the chance for the unfavourably oriented grains to be further refined into equiaxed grains. In Ref [27], an Al-4 wt.% Cu alloy

deformed to a strain of ~10 via route A using a 120˚ ECAP die exhibited a submicron-sized lamellar grain structure. In the present work, a different grain structure was obtained. This result should be attributed to the fact that a 90˚ die was used in the present work, which can generate more shear bands and enhance the formatiom of equiaxed grains. Lastly, the coarse Al_2Cu particles along the grain boundaries also contribute to the inhomogerous deformation and the grain refinement [20]. The high misorientation gradient of the matrix in the vicinity of the coarse particles, promotes the CDRX process and thus the formation of equiaxed UFG grains.

3.2. Mechanical properties

3.2.1. Hardness

The evolution of Vickers hardness with increasing number of passes is shown in Fig. 6(a). As shown, the hardness increases sharply after one pass, i.e. from 77 HV in the initial as-homogenized state to 125 HV, followed by a relatively slow increase rate during the 2nd, 3rd and 4th pass, finally reaching 147 HV which is about 2 times the hardness of the as-homogenized state. The slower hardness increase rate at higher deformation strains can be attributed to the gradual supersaturation of dislocations in the coarse grains.

3.2.2. Tensile properties

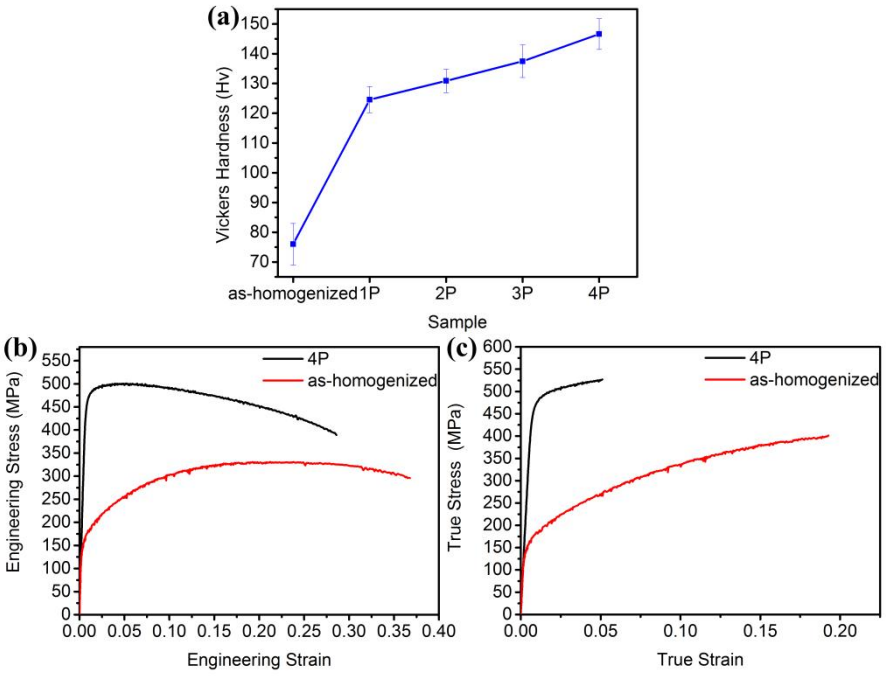

Fig. 6. Mechanical properties of the 4P sample. (a) Evolution of Vickers hardness with increasing ECAP passes, (b) engineering stress-strain curves and (c) true stress-strain curves.

Typical engineering stress-strain and true stress-strain curves for the as-homogenized and 4P samples are shown in Fig. 6(b) and (c), respectively. The corresponding mechanical properties, i.e., yield strength (YS), ultimate tensile strength (UTS) and elongation, are summarized in Table 1. For comparison, some tensile property results of Al-Cu alloys processed by ECAP reported in different literatures are also included in Table 1. The as-homogenized samples exhibit a moderate strength, i.e. YS of ~169 MPa and UTS of ~331 MPa. A substantial strength improvement was achieved in the 4P sample, i.e. YS of ~457 MPa and UTS of ~501 MPa.

Table 1. Tensile properties of the as-homogenized and the 4P samples. For comparison, data for room-temperature ECAP processed Al-Cu alloys reported in different literatures are also included.

Material	Die (equivalent strain per pass)	Equivalent strain	Yield strength (0.2% offset) (σ_{ys}) [MPa]	Ultimate tensile stress [MPa]	Elongation to failure (ε_f) [%]	Uniform elongation (ε_u) [%]
Al-5 wt.% Cu (as-homogenized, this work)	-	-	169	331	36.8	21.2
Al-5 wt.% Cu (this work)	Φ = 90˚, (1)	4	457	501	28	5
Al-5 wt.% Cu [18]	Φ = 110˚, (0.77)	6.16	~350	~ 493	~ 8	-
Al-4.1 wt.% Cu [28]	Φ = 120˚, (0.67)	2.68	442	460	7.9	0.9
Al-4.1 wt.% Cu (with post-ECAP annealing at 170 ℃ for 2 hours) [28]	Φ = 120˚, (0.67)	2.68	328	368	8.0	3.0
Al-3.9 wt.% Cu [15]	Φ = 90˚, (1)	4	-	290	2.7	-
Al-3 wt.% Cu [29]	Φ = 110˚, (0.77)	6.16	-	445	-	-

The high strength of the UFG Al-5Cu achieved by four passes of ECAP in this work can be attributed to three factors, i.e. solid solution strengthening by a high solute content of Cu, strengthening by a high dislocation density and grain boundary strengthening due to the decrease of grain size.

In the present work, the average equivalent circular grain size of the 4P Al-5Cu sample was ~0.5 μm. According to the the classical Hall-Petch (HP) relationship $\Delta\sigma_{GB} = kd^{-1/2}$, where σ is the yield strength, d is the average grain size and k is a material-dependent constant (here k is taken as 130 MPa $\mu m^{1/2}$ [30]), the increase of strength by grain refinement is estimated to be ~184 MPa for the 4P sample (vs. ~20 MPa for the as-homogenized sample).

According to classical work hardening theories, the strength contribution from dislocation-dislocation interactions is given by the following relationship: $\Delta\sigma_d = M\alpha Gb\sqrt{\rho}$ [31], where α is a numerical constant measuring the efficiency of dislocation strengthening, G is the shear modulus, and b is the Burgers vector. The larger increase in YS than UTS in comparison to the as-homogenized material indicates a reduction in

work hardening capability of ECAP processed materials. This is because the dislocation density of the ECAP processed sample is already high and therefore cannot further increase at the same rate as that of the as-homogenized alloy during tensile testing. According to the difference of the yield strength between the as-homogenized and 4P samples, the value of strengthening owing to work hardening in the 4P sample can be estimated to be $\Delta\sigma_d = 457 - 169 + 20 - 184 = 104$ MPa. Here we can also estimate the dislocation density of the 4P sample by taking $\alpha = 0.3$, G = 27 GPa, b = 2.86×10^{-10} m and the Taylor factor M=3 [13]. Applying the estimated value of $\Delta\sigma_d = 84$ MPa gives a dislocation density of $\sim 1.5 \times 10^{14}$ m^{-2}, which compares well with the estimated value based on the misorientation gradient.

Among different mechanical properties of UFG materials processed by SPD, ductility is particularly important since it relates to fracture toughness and formability. The strain prior to the onset of necking is an indispensable value in the formability of sheet metal because its magnitude specifies the permissible strain to obtain uniform or homogeneous deformation (ε_u), after which local thinning (i.e., inhomogeneous deformation) may occur. In addition to the significance of ε_u on formability, the total elongation (ε_f) at fracture is also being considered as an essential indicator of formability. Here, $\varepsilon_f = \varepsilon_u + \varepsilon_{pu}$, where ε_{pu} is the post-uniform elongation. After four passes, the values of ε_u and ε_f reached 5% and 28%, respectively.

Although the uniform elongation of the 4P sample is much reduced in comparison to the as-homogenized state, it is significantly larger than previously reported values of ECAP processed Al-Cu (containing 3-5 wt.% Cu) alloys, and even superior to that of the Al-4.1 wt.% Cu alloy with post-ECAP annealing at 170℃ for 2 hours (see Table 1). It is well known that the work hardening ability is important for stabilizing uniform tensile deformation. In this study, the enhanced work hardening can be interpreted in light of the high solute content of Cu and the bimodal grain structure.

During tensile deformation, non-uniform deformation starts when the condition predicted by the Considère criterion is reached, $(\frac{\partial\sigma}{\partial\varepsilon})_{\dot{\varepsilon}} \leq \sigma$, where σ and ε are true stress and true strain, respectively, and $\dot{\varepsilon}$ is the strain rate. Typically, the strength of heavily deformed metals is high and work hardening rate is low, making it easy for inhomogeneous deformation to onset at small strains. Thus, an increase of work hardening rate can postpone the onset of instability of plastic flow, resulting in a large uniform elongation. A dynamic balance between dislocation generation and annihilation determines the work hardening rate, while the uniform strain during tensile deformation is primarily controlled by the rate of dynamic recovery

[32]. In this study, the high Cu solute contents can retard the annihilation of dislocations by pinning the migration of mobile dislocations and accordingly, the ECAP processed material can reach a higher supersaturating density of dislocations, resulting in a high work hardening rate, thus improving the uniform elongation.

Furthermore, the interior of coarse grains has a much lower dislocation density than those areas adjacent to the HABs, which means that coarse grains have ample space for accommodating newly generated dislocations during the tensile deformation. Thus, the micron-sized (large) grains increase the work hardening capacity. Additionally, the coarse grains themselves not only participate in the plastic deformation but also help release the stress concentration in the UFG matrix [12]. Crack propagation across these large and ductile grains dissipates a considerable amount of energy [28], thereby delaying crack initiation and propagation. This bimodal microstructure is supposed to be the most important reason for the large uniform elongation and post-uniform elongation in the 4P sample.

3.2.3 Fracture of tensile samples

Detailed fracture morphology of the tensile specimens was obtained by using SEM. As indicated in Fig. 7(a), the as-homogenized sample shows a typical dimple-like ductile fracture, where the diameter of the dimples is measured as ~12-25 μm. The fracture surfaces of the 4P sample are shown in Fig. 7(b)~(d). As can be seen, the dimples in the 4P sample are generally shallow and the size varies a lot. Two distinctive features are noted for the dimples. The first one is the large areas of a poorly defined dimple morphology (marked by an oval circle in Fig. 7(b)), which is supposed to be correlated to ultrafine grained regions. In metals containing ultrafine grains, the dimensions of the dimple-like features observed on the fracture surface are usually considerably larger than the grain sizes [33-35]. The reason is that since fracturing of UFG grains operates at a larger scale and eventually involve collective grain activity [33]. Based on Fig. 7(b), it seems that a considerable fraction of grains (~70% in area fraction) is in the UFG range. The second feature of the fracture surface is the well-defined deeper dimples associated with the CG regions, which are similar to those seen in the as-homogenized sample. These dimples indicate that some plastic deformation has occurred prior to fracture, which contributes to the improved elongation to failure. Atomistic simulations of crack propagation in NC materials have demonstrated that inter-granular fracture proceeded by coalescence of micro-voids ahead of the crack [36]. According to the model by Lavernia and

collaborators [37, 38], cracks follow a fast and intergranular path when running through the nanostructured grains, but are blunted and slowed down when they encounter a large and soft grain. The coarse grains in a bimodal grain structure are therefore an important reason to attain large uniform elongation in the 4P sample.

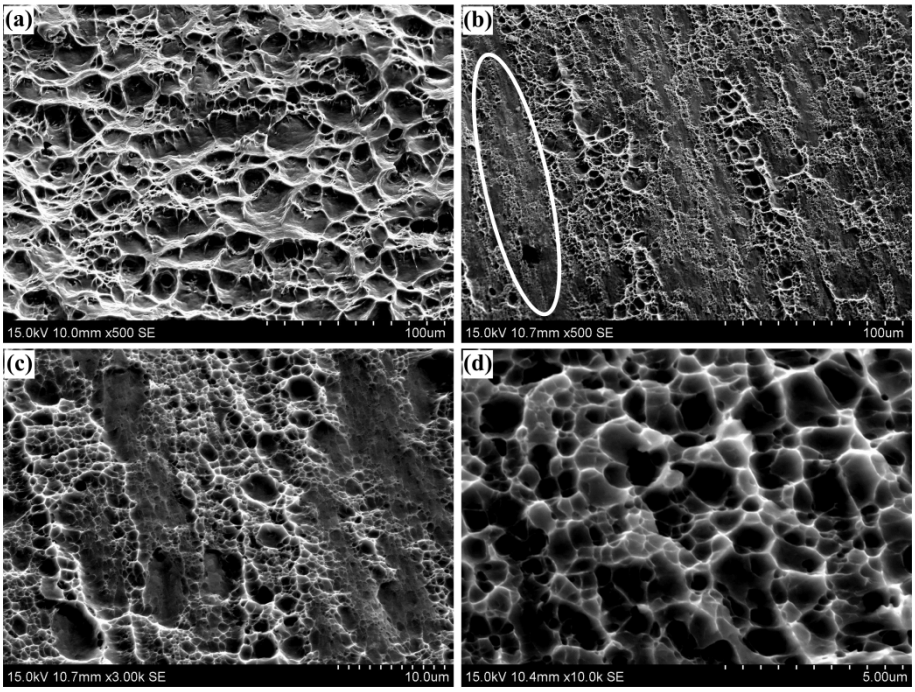

Fig. 7. Fracture morphologies of Al-5Cu alloy. (a) as-homogenized; (b), (c) and (d) 4P.

4. Conclusions

The microstructural evolution and mechanical properties of an ECAP processed Al-5wt.% Cu alloy containing a small fraction of Al_2Cu eutectic particles were investigated. The microstructure analysis revealed that during ECAP, the grain refinement occurs predominantly by subdivision of original coarse grains by forming shear bands and by continuous dynamic recrystallization (CDRX). The coarse eutectic Al_2Cu particles along grain boundaries can enhance the formation of UFG grains around the particles. Due to the high solute content of Cu and ECAP via route A, some of the coarse grains are difficult to be refined into UFG grains. As a consequence, a bimodal grain structure can be achieved after four passes of ECAP. Tensile tests showed that high strength (UTS ≈ 500 MPa) and good ductility (i.e. elongation to failure ~28% and uniform elongation ~5%) can be achieved simultaneously in the ECAP Al-5Cu alloy. High yield strength is a combination of different strengthening mechanisms, i.e. solid solution strengthening by a high content of Cu, strain hardening by a high dislocation density, and grain boundary strengthening. The high

solute content of Cu and the bimodal grain structure is supposed to lead to the enhanced rate and capacity of work hardening, respectively, resulting in the improved uniform elongation. The results of the present work suggest a new strategy for designing and manufacturing UFG metal alloys with both high strength and good ductility.

Acknowledgements

The authors would like to acknowledge the financial support from Research Council of Norway, under the FRINATEK project 'BENTMAT' (Project number 10407002) and China Scholarship Council (201406080011). The authors also greatly appreciate the assistance of Mr. Pål C. Skaret during ECAP experiments and tensile tests.

References

[1] R.Z. Valiev, R.K. Islamgaliev, I.V. Alexandrov, Bulk nanostructured materials from severe plastic deformation, Progress in Materials Science 45 (2000) 103-189.
[2] Y. Iwahashi, J. Wang, Z. Horita, M. Nemoto, T.G. Langdon, Principle of equal-channel angular pressing for the processing of ultra-fine grained materials, Scripta Materialia 35 (1996) 143-146.
[3] Y. Iwahashi, M. Furukawa, Z. Horita, M. Nemoto, T. Langdon, Microstructural characteristics of ultrafine-grained aluminum produced using equal-channel angular pressing, Metallurgical and Materials Transactions A 29 (1998) 2245-2252.
[4] M. Furukawa, Z. Horita, M. Nemoto, T.G. Langdon, Review: Processing of metals by equal-channel angular pressing, Journal of Materials Science 36 (2001) 2835-2843.
[5] M. Furukawa, Z. Horita, T.G. Langdon, Factors influencing the shearing patterns in equal-channel angular pressing, Materials Science and Engineering: A 332 (2002) 97-109.
[6] C.C.Koch, Optimization of strength and ductility in nanocrystalline and ultrafine grained metals, Scr. Mater. 49 (2003) 657-662.
[7] Y.H. Zhao, Y.T. Zhu, X.Z. Liao, Z. Horita, T.G. Langdon, Tailoring stacking fault energy for high ductility and high strength in ultrafine grained Cu and its alloy, Applied Physics Letters 89 (2006) 121906.
[8] Z. Horita, K. Ohashi, T. Fujita, K. Kaneko, T.G. Langdon, Achieving High Strength and High Ductility in Precipitation-Hardened Alloys, Advanced Materials 17 (2005) 1599-1602.
[9] Y.M. Wang, E. Ma, Three strategies to achieve uniform tensile deformation in a nanostructured metal, Acta Materialia 52 (2004) 1699-1709.
[10] S. Nelson, L. Ladani, T. Topping, E. Lavernia, Fatigue and monotonic loading crack nucleation and propagation in bimodal grain size aluminum alloy, Acta Materialia 59 (2011) 3550-3570.
[11] A. Magee, L. Ladani, T.D. Topping, E.J. Lavernia, Effects of tensile test parameters on the mechanical properties of a bimodal Al–Mg alloy, Acta Materialia 60 (2012) 5838-5849.
[12] G.J. Fan, H. Choo, P.K. Liaw, E.J. Lavernia, Plastic deformation and fracture of ultrafine-grained Al–Mg alloys with a bimodal grain size distribution, Acta Materialia 54 (2006) 1759-1766.
[13] M. Zha, Y. Li, R.H. Mathiesen, R. Bjørge, H.J. Roven, Microstructure evolution and mechanical behavior of a binary Al–7Mg alloy processed by equal-channel angular pressing, Acta Materialia 84 (2015) 42-54.

[14] M. Zha, Y. Li, R.H. Mathiesen, R. Bjørge, H.J. Roven, High ductility bulk nanostructured Al-Mg binary alloy processed by equal channel angular pressing and inter-pass annealing, Scripta Mater. 105 (2015) 22-25.
[15] D.R. Fang, Z.F. Zhang, S.D. Wu, C.X. Huang, H. Zhang, N.Q. Zhao, J.J. Li, Effect of equal channel angular pressing on tensile properties and fracture modes of casting Al–Cu alloys, Materials Science and Engineering: A 426 (2006) 305-313.
[16] D.R. Fang, Y.Z. Tian, Q.Q. Duan, S.D. Wu, Z.F. Zhang, N.Q. Zhao, J.J. Li, Effects of equal channel angular pressing on the strength and toughness of Al–Cu alloys, Journal of Materials Science 46 (2011) 5002-5008.
[17] E. Prados, V. Sordi, M. Ferrante, Tensile behaviour of an Al–4 wt.%Cu alloy deformed by equal-channel angular pressing, Materials Science and Engineering: A 503 (2009) 68-70.
[18] N. El Mahallawy, F.A. Shehata, M.A. El Hameed, M.I.A. El Aal, Effect of Cu content and number of passes on evolution of microstructure and mechanical properties of ECAPed Al/Cu alloys, Materials Science and Engineering: A 517 (2009) 46-50.
[19] M. El Aal, N. El Mahallawy, F. Shehata, M. El Hameed, E. Yoon, J. Lee, H. Kim, Tensile properties and fracture characteristics of ECAP-processed Al and Al-Cu alloys, Metals and Materials International 16 (2010) 709-716.
[20] M. Berta, P.J. Apps, P.B. Prangnell, Effect of processing route and second phase particles on grain refinement during equal-channel angular extrusion, Materials Science and Engineering: A 410–411 (2005) 381-385.
[21] P.J. Apps, J.R. Bowen, P.B. Prangnell, The effect of coarse second-phase particles on the rate of grain refinement during severe deformation processing, Acta Materialia 51 (2003) 2811-2822.
[22] R.Z. Valiev, T.G. Langdon, Principles of equal-channel angular pressing as a processing tool for grain refinement, Progress in Materials Science 51 (2006) 881-981.
[23] D.A. Hughes, Microstructural evolution in a non-cell forming metal: Al-Mg, Acta Metallurgica et Materialia 41 (1993) 1421-1430.
[24] V. Gerold, H.P. Karnthaler, On the origin of planar slip in f.c.c. alloys, Acta Metall. 37 (1989) 2177-2183.
[25] S.I. Hong, C. Laird, Mechanisms of slip mode modification in F.C.C. solid solutions, Acta Metall. Mater. 38 (1990) 1581-1594.
[26] W.Z. Han, Z.F. Zhang, S.D. Wu, S.X. Li, Influences of crystallographic orientations on deformation mechanism and grain refinement of Al single crystals subjected to one-pass equal-channel angular pressing, Acta Materialia 55 (2007) 5889-5900.
[27] Y. Huang, J.D. Robson, P.B. Prangnell, The formation of nanograin structures and accelerated room-temperature theta precipitation in a severely deformed Al–4wt.% Cu alloy, Acta Materialia 58 (2010) 1643-1657.
[28] E.F. Prados, V.L. Sordi, M. Ferrante, The effect of Al_2Cu precipitates on the microstructural evolution, tensile strength, ductility and work-hardening behaviour of a Al–4 wt.% Cu alloy processed by equal-channel angular pressing, Acta Materialia 61 (2013) 115-125.
[29] M.I.A.E. Aal, Influence of the pre-homogenization treatment on the microstructure evolution and the mechanical properties of Al–Cu alloys processed by ECAP, Materials Science and Engineering: A 528 (2011) 6946-6957.
[30] T. Shanmugasundaram, M. Heilmaier, B.S. Murty, V.S. Sarma, On the Hall–Petch relationship in a nanostructured Al–Cu alloy, Materials Science and Engineering: A 527 (2010) 7821-7825.
[31] H. Mecking, U.F. Kocks, Kinetics of flow and strain-hardening, Acta Metall. 29 (1981) 1865-1875.
[32] A. Vinogradov, I.S. Yasnikov, H. Matsuyama, M. Uchida, Y. Kaneko, Y. Estrin, Controlling strength and ductility: Dislocation-based model of necking instability and its verification for ultrafine grain 316L steel, Acta Materialia 106 (2016) 295-303.
[33] A. Hasnaoui, H. Van Swygenhoven, P.M. Derlet, Dimples on Nanocrystalline Fracture Surfaces As Evidence for Shear Plane Formation, Science 300 (2003) 1550-1552.

[34] Y.M. Wang, E. Ma, M.W. Chen, Enhanced tensile ductility and toughness in nanostructured Cu, Applied Physics Letters 80 (2002) 2395-2397.
[35] K.S. Kumar, S. Suresh, M.F. Chisholm, J.A. Horton, P. Wang, Deformation of electrodeposited nanocrystalline nickel, Acta Materialia 51 (2003) 387-405.
[36] D. Farkas, H. Van Swygenhoven, P. Derlet, Intergranular fracture in nanocrystalline metals, Physical Review B 66 (2002) 060101.
[37] V.L. Tellkamp, E.J. Lavernia, A. Melmed, Mechanical behavior and microstructure of a thermally stable bulk nanostructured Al alloy, Metallurgical and Materials Transactions A 32 (2001) 2335-2343.
[38] B.O. Han, E.J. Lavernia, Z. Lee, S. Nutt, D. Witkin, Deformation behavior of bimodal nanostructured 5083 Al alloys, Metallurgical and Materials Transactions A 36 (2005) 957-965.

Tables.

Table 1. Tensile properties of the as-homogenized and the 4P samples. For comparison, data for room-temperature ECAP processed Al-Cu alloys reported in different literatures are also included.

Figure captions.

Fig. 1. Microstructure of the original as-homogenized Al-5Cu alloy: (a) EBSD map and (b) BSE map.

Fig. 2. Microstructures of the 1P sample: (a) BSE image; (b) EBSD image corresponding to the area within the white rectangular frame in (a); (c) enlarged EBSD image of the selected grain GI, showing diffuse boundaries; (d) selected grain GII, showing micro-bands. Corresponding misorientation profiles measured along the lines are also included. Inside of GI and GII, the blue and red lines depict differences between neighbouring grid points $2^\circ < \Theta \leq 5^\circ$ and $5^\circ < \Theta \leq 15^\circ$ respectively.

Fig. 3. Typical BSE images, and corresponding EBSD maps of the areas indicated by rectangular frames in the BSE images. (a) and (b) 2P; (c) and (d) 3P; (e) and (f) 4P. The white dots in the BSE images are eutectic Al_2Cu particles. In the EBSD maps, narrow grey and coarse black lines depict differences between neighbouring grid points $5^\circ < \Theta \leq 15^\circ$ and $15^\circ < \Theta \leq 180^\circ$ respectively.

Fig. 4. The evolution of (a) the average crystallite size with boundary misorientation $\geq 5^\circ$, (b) fraction of different boundaries and (c) average misorientation of boundaries as a function of equivalent deformation strain; (d) grain size distribution of the 4P sample.

Fig. 5. (a) and (c) Typical ASTAR-TEM orientation images of the 4P sample and the step sizes are 10.2 nm and 9.0 nm, respectively. The narrow grey and coarse black lines depict LABs ($5^\circ < \Theta < 15^\circ$) and HABs ($15^\circ < \Theta < 180^\circ$), respectively. (b) and (d) Representative TEM images of the 4P sample, where (b) is taken from the framed area in (a).

Fig. 6. Mechanical properties of the 4P sample. (a) Evolution of Vickers hardness with increasing ECAP passes, (b) engineering stress-strain curves and (c) true stress-strain curves.

Fig. 7. Fracture morphologies of Al-5Cu alloy. (a) as-homogenized; (b), (c) and (d) 4P.